Measurement Module of Dispersion Interferometer Based on the CO$_2$ Laser for Plasma Density Control

S. V. Ivanenko[a,*], K. A. Grinemayer[a], E. A. Puryga[a], A. N. Kvashnin[a], and P. A. Bagryansky[a]

[a]*Budker Institute of Nuclear Physics, Siberian Branch, Russian Academy of Sciences, Novosibirsk, 630090 Russia*
* e-mail: ivanenko.sveta@gmail.com

Abstract—This article discusses a measurement module of a dispersion interferometer based on a CO$_2$ laser for integral plasma density measurements with a resolution of 4×10^{11} cm^{-2} with a time discreteness of 4 μs. Such characteristics of the device make it possible to use the results of its measurements in feedback loops for plasma density control. The main elements of the measurement module are crystals of analog-to-digital converters (ADCs) and a digital streaming data processing node based on a field-programmable gate array (FPGA). The algorithm for calculating the plasma density implemented in the digital node is based on the harmonic analysis of interferometer signals and is resistant to noise and changes in the modulation depth. The measurement module under consideration is a prototype of the system of monitoring and automatic control of plasma density at the Globus-M2 facility (St. Petersburg, Russia).

INTRODUCTION

Interferometry is a classical method of plasma density diagnostics in modern thermonuclear facilities. This method makes it possible to obtain an absolute value of the electron density integral of plasma along the observation line, because the phase difference which it measures depends only on the density, the characteristic size of the plasma, and the world constants. This property of interferometry is widely used to calibrate other diagnostics and to understand the general aspects of plasma behavior, and, most importantly, it can be used to generate feedback signals in modern systems for dynamic stabilization of density and plasma filament position in magnetic traps. At the same time, the very possibility of hardware implementation of such plasma density control has become available largely through the development of microelectronics and the appearance on the market of digital streaming data processing tools, such as field-programmable gate arrays (FPGAs). The presence of a FPGA-based digital core in the used monitoring equipment makes it possible to fully transfer the process of calculating the plasma density directly to the monitoring modules themselves. In this case, the results will be generated in real time. This fact makes it possible to use the obtained results in feedback loops and to create a system for automatic control of plasma density.

The features of the dispersion interferometer (DI) based on a CO$_2$ laser with an artificial phase modulation of the probing radiation [1] used in this work are its compactness and weak sensitivity to vibrations of optical elements. The DI scheme (Fig. 1) uses wavelength separation of probing beams owing to partial conversion of the initial radiation of the first harmonic into the second one; the measurement principle is based on the analysis of the phase shift between these beams in plasma. Owing to the choice of the optimal wavelength for modern plasma generators (5 and 10 μm), the operation of this interferometer is almost unaffected by the phenomena of refraction and rotation of the plane of polarization in the magnetic field.

Similar interferometers are used at the GDL (Novosibirsk, Russia) [1], W-7X (Greifswald, Germany) [2], and LHD facilities (Toki, Japan) [3], and one was also previously used at the TEXTOR facility (Jülich, Germany) [4]. In order to detect signals and calculate the plasma density, different methods were used in these interferometers, and special measuring instruments were created. In particular, a measuring complex was created at the TEXTOR facility, which made it possible not only to measure the integral plasma density in real time but also to control the plasma density and the vertical position of the plasma toroid [5, 6]. Despite the successful implementation, the method of calculating the plasma density described in [6] was unstable to the noise superim-
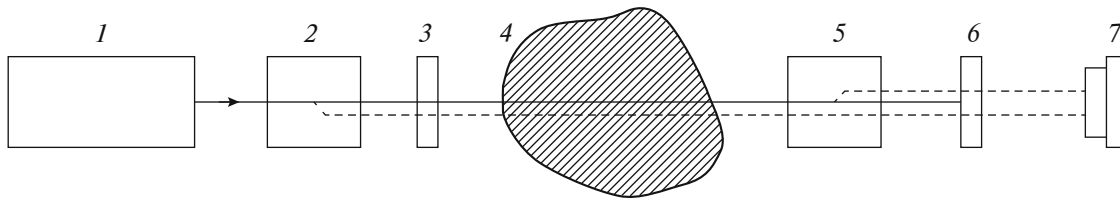
Fig. 1. Schematic diagram of the DI with an electro-optical cell included in it: (*1*) CO_2 laser; (*2* and *5*) frequency doublers; (*3*) electro-optical cell; (*4*) plasma; (*6*) filter; and (*7*) photodetector.

posed on the signal and changes in the modulation depth. All this forced one to carry out cumbersome calibration procedures before calculating each new value of the plasma density. In recent years, the main approach to solving the problem of calculating the plasma density was to work with the interferometer signal in the frequency domain rather than in the time domain [7]. This made it possible to significantly reduce the susceptibility of the results to noise and get rid of cumbersome calibration procedures.

This article describes the DI measurement module, which is a prototype of the system for monitoring and automatic control of plasma density at the Globus-M2 facility (St. Petersburg, Russia) [8]. It is based on the DI measurement complex for the TEXTOR and GDL facilities described in [6]. By using fundamentally new algorithms for calculating the plasma density based on the harmonic analysis, it became possible not only to increase the measurement accuracy in the presence of noise and get rid of the calibration procedures but also to provide robustness against the changes in the modulation depth of the interferometer signal.

PHASE EXTRACTION ALGORITHM

In the classical DI scheme, the photodetector signal has the form [9]

$$I = I_1 + I_2 + 2\sqrt{I_1 I_2} \sin(\Delta\varphi), \qquad (1)$$

where I_1 and I_2 are the intensities of probing and reference waves, and $\Delta\varphi$ is their phase difference proportional to the integral plasma density $\int n_e dl$ and related to it by the expression

$$\Delta\varphi = \frac{3}{2}\frac{e^2}{mc^2}\lambda\int_0^L n_e dl. \qquad (2)$$

In this relation, the electron charge e, electron mass m, speed of light c, and wavelength of probing radiation λ play the role of scale factors. In order to increase the sensitivity of the interferometer, an electro-optical (EO) cell was added to its circuit. Under the influence of the applied sinusoidal voltage, it artificially changes the phase shift of the radiation passing through it. As a result, an oscillating component appears in the argument of the function describing the DI output signal:

$$I = I_1 + I_2 + 2\sqrt{I_1 I_2} \sin(M \sin(\Omega t) + \Delta\varphi). \qquad (3)$$

With its amplitude M of π or more radians, the output signal changes from maximum to minimum regardless of the phase shift $\Delta\varphi$ caused by the plasma.

There are several methods for hardware extraction of the phase shift $\Delta\varphi$. In particular, study [6] used an algorithm that works with the photodetector and modulator signals in the amplitude–time domain. Assuming that the intensities of the probing and reference waves I_1 and I_2 are fixed by the modulation period, the constant component was excluded from the photodetector signal, and its variable component was normalized to unity. In this case, the current phase shift at the points where the sine function argument is zero, corresponding to the points of maximum interferometer sensitivity, is directly proportional to the current value of the modulating signal amplitude:

$$\Delta\varphi = |M \sin(\Omega t)|. \qquad (4)$$

Despite the simplicity of implementation, this method had a number of drawbacks. First of all, there is a strong dependence of the measurement results on the noise superimposed on the signal. The main sources of noise affecting the amplitude of the photodetector signal include the following:

— Instability of the laser output power.

— Instability of temperature and orientation of the nonlinear crystal.

— Instability of the total transmittance of the optical path taking into account dusting of the mirror surfaces facing the plasma and other effects.

— Large-scale transverse beam shifts comparable with the apertures of the detector and other limiting optical elements.

Such phenomena can occur owing to refraction at sharp density gradients (e.g., in the case of plasma disruptions in a tokamak) or in the case of large amplitude vibrations (also occurring during disruptions).

In addition, the following factors directly affect the measurement results and lead to a change in the photodetector signal shape:

— Insufficient or excessive modulation depth of the probing radiation.

— Additional phase shift in the EO cell due to temperature instability, acoustic resonances, or other reasons.

— Parasitic feedback between the laser and the interferometer optical system. Such an effect arises owing to the reflected radiation from various optical elements hitting the laser, its amplification in the laser, and subsequent interference with the main radiation.

— Phase jump during laser realignment to an adjacent generation line in the group.

While the problems of signal amplitude fluctuations could have been solved by adding auxiliary calibration procedures to the processing algorithm, it was impossible to take into account changes in the modulating signal depth in the process of facility operation in the same way. As a result, all this led to errors in measurements of the phase shift and, accordingly, the plasma density. Therefore, when developing a prototype of the system of monitoring and automatic control of plasma density at the Globus-M2 facility, it was decided to switch from the amplitude–time domain to the amplitude–frequency domain. The algorithm described in [7] was taken as the basis.

After conversion to the voltage at the photodetector, intensity signal (3) has the form

$$V(t) = V_{DC} + V_{AC}\cos[M\sin(\Omega t + \Delta\varphi)]. \quad (5)$$

Trigonometric expansion of the cosine gives

$$V(t) = V_{DC} + V_{AC}\{\cos(\Delta\varphi)\cos[M\sin(\Omega t)] \\ - \sin(\Delta\varphi)\sin[M\sin(\Omega t)]\}. \quad (6)$$

Let us use the identities

$$\cos[M\sin(\Omega t)] \\ = J_0(M) + 2\sum_{n=1}^{\infty} J_{2n}(M)\cos[(2n)\Omega t]; \quad (7)$$

$$\sin[M\sin(\Omega t)] = 2\sum_{m=1}^{\infty} J_{2m-1}(M)\sin[(2m-1)\Omega t], \quad (8)$$

where $J_n(x)$ is a Bessel function of the first kind of order n. Substituting (7) and (8) into (6) results in a harmonic expansion of the signal:

$$V(t) = [V_{DC} + V_{AC}\cos(\Delta\varphi)J_0(M)] \\ - 2V_{AC}\sin(\Delta\varphi)J_1(M)\sin(\Omega t) \\ + 2V_{AC}\cos(\Delta\varphi)J_2(M)\cos(2\Omega t) \quad (9) \\ - 2V_{AC}\sin(\Delta\varphi)\sum_{m=2}^{\infty} J_{2m-1}(M)\sin[(2m-1)\Omega t] \\ + 2V_{AC}\cos(\Delta\varphi)\sum_{n=2}^{\infty} J_{2n}(M)\cos[(2n)\Omega t].$$

We turn our attention to the first and second harmonics $V(t)$:

$$V_{\Omega}(t) = -2V_{AC}\sin(\Delta\varphi)J_1(M)\sin(\Omega t);$$

$$V_{2\Omega}(t) = 2V_{AC}\cos(\Delta\varphi)J_2(M)\cos(2\Omega t).$$

These two frequency components contain sufficient information to uniquely identify $\Delta\varphi$. By taking the ratio of their amplitudes, we can eliminate the dependence on V_{AC}:

$$\frac{J_2(M)}{J_1(M)}\frac{V_{\Omega}(t)}{V_{2\Omega}(t)} = \frac{|\sin(\Delta\varphi)|}{|\cos(\Delta\varphi)|} = |\tan(\Delta\varphi)|. \quad (10)$$

Therefore, we find that the phase difference $\Delta\varphi$ depends only on the amplitudes of the first and second harmonics of the photodetector signal and the amplitude of the modulating signal. Using the arctangent function, we can reconstruct $\Delta\varphi$ in the interval $[0, \pi/2]$.

Modulation Depth Consideration

The expression to determine phase difference (10) contains two unknown ratios $\left|\frac{J_2(M)}{J_1(M)}\right|$ and $\left|\frac{V_{\Omega}(t)}{V_{2\Omega}(t)}\right|$. The need to calculate the ratio $\frac{J_2(M)}{J_1(M)}$ (rather than taking it as a constant) is due to the fact that the modulation depth M, as already mentioned, is not a constant value and can vary because of temperature effects on the modulation ratio of the GaAs crystal used in the EO cell. In the used DI, the value of the modulation depth is in the range from $\pi/2$ to π and is determined by the voltage of the EO cell.

According to (9), we have the following expressions for the first and third harmonics:

$$V_{\Omega}(t) = -2V_{AC}\sin(\Delta\varphi)J_1(M)\sin(\Omega t);$$

$$V_{3\Omega}(t) = -2V_{AC}\sin(\Delta\varphi)J_3(M)\sin(3\Omega t).$$

By taking the ratio of their amplitudes, we can determine the current depth of modulation using the pregenerated table of M values depending on $\frac{J_1(M)}{J_3(M)}$:

$$\left|\frac{V_{\Omega}(t)}{V_{3\Omega}(t)}\right| = \left|\frac{J_1(M)}{J(M)}\right|. \quad (11)$$

And then we can calculate the ratio $\frac{J_2(M)}{J_1(M)}$ needed for (10).

Therefore, the calculation of the modulation depth at every period of the modulating signal and considering it when calculating the current phase value $\Delta\varphi$ make it possible to get rid of an additional source of error and to improve significantly the measurement accuracy.

Table 1. Determining the quadrant for the phase shift by harmonic signs

Harmonic	$V_{2\Omega}+$	$V_{2\Omega}-$
$V_{\Omega}+$	I	II
$V_{\Omega}-$	IV	III

Extension of the Phase Measurement Range

Expression (10) makes it possible to determine the phase $\Delta\varphi$ only in the range from 0 to $\pi/2$. In order to extend this range, additional information is needed, which can be the signs of the first two harmonics of the photodetector signal:

$$V_{\Omega}(t) = -2V_{AC}\sin(\Delta\varphi)J_1(M)\sin(\Omega t);$$

$$V_{2\Omega}(t) = 2V_{AC}\cos(\Delta\varphi)J_2(M)\cos(2\Omega t).$$

Owing to the fact that the Bessel functions J_1 and J_2 are positive in the $\pi \pm \pi/6$ region, only the cosine and sine phase functions affect the sign. The position of the phase quadrant depending on the signs of the harmonics is shown in Table 1.

At high plasma densities, the phase shift can exceed 360°. Because of the periodicity of the cosine (expression (6)), the phase shift occurs at this boundary, resulting in a loss of information about the full phase arrival. This feature imposes a limit on the phase shift rate: no more than 90° per modulation period (4 µs). This corresponds to a change in the average linear density of $\approx 4 \times 10^{15}$ cm^{-2}, which in turn corresponds to a change in plasma density of 4×10^{13} cm^{-3} in 4 µs at a characteristic length of 1 m. This is several times greater than the changes in density observed at modern plasma facilities under normal conditions [10]. If necessary, this limitation can be overcome by using a shorter wavelength laser or a higher modulation frequency.

DISPERSION INTERFEROMETER MEASUREMENT MODULE

In order to implement the described algorithm, a special measurement module (phasemeter) was developed (Fig. 2). Signals from the photodetector and modulator of the EO cell with a frequency of 250 kHz are fed to the input of the phasemeter. These signals are digitized by 14-bit ADCs (AD9255) with a sampling rate of 64 MHz. From the ADC outputs, a sequence of digital samples is transmitted to the digital processing node based on an Intel Cyclone 3 FPGA. This node is responsible for the implementation of the phase shift extraction algorithm, the generation of the reference frequency (250 kHz) for the modulator of the EO cell, the recording into memory (RAM), and further transfer of measurement results to a Colibri iMX6 processor module, which is based on an ARM processor and runs under the Linux operating system. The processor module is responsible for data transmission via an Ethernet channel to the diagnostic server and for receiving control commands from the server, such as selection of the operating mode and selection of the program or external start.

The phasemeter supports two operating modes: measuring and oscillographic. In the measuring mode, the signals are processed, and the integral plasma density is calculated in real time with subsequent recording of the measurement results in RAM (the maximum duration of the registration cycle is 8 s). In the oscillographic mode, the readings from both
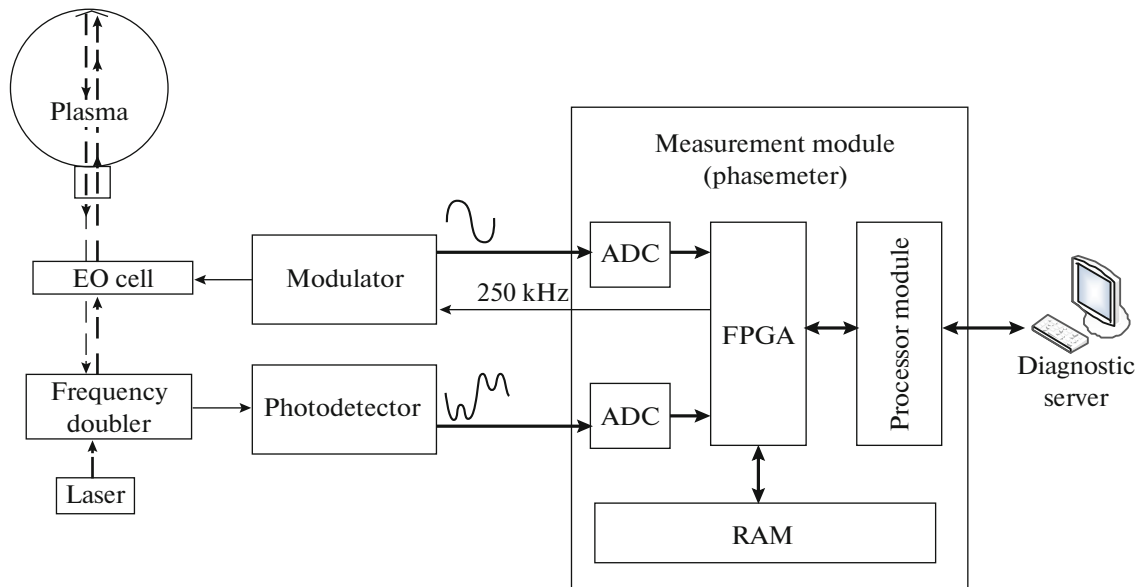
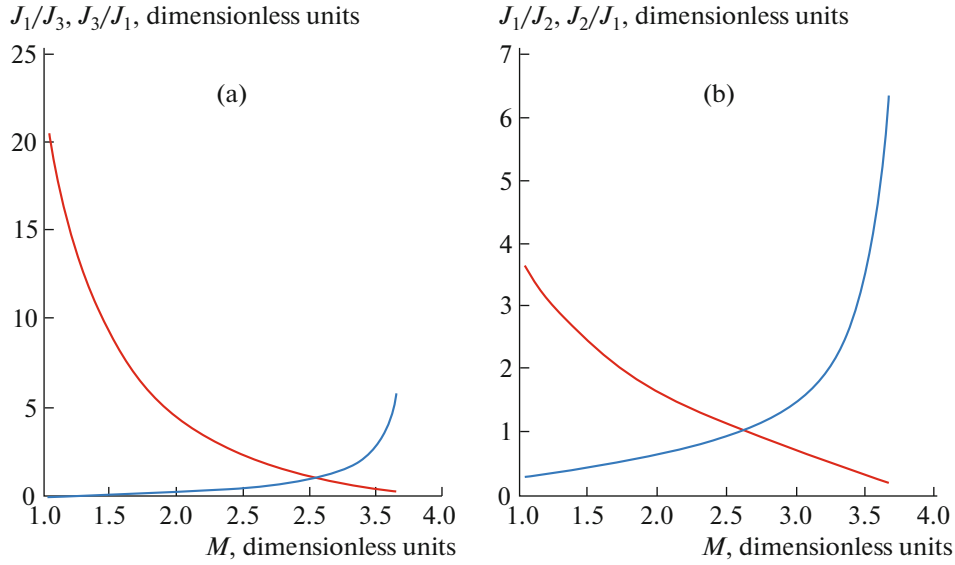**Fig. 2.** Measurement module as a part of dispersion interferometer.

Fig. 3. (a) Ratios J_1/J_3 (——) and J_3/J_1 (——) depending on the modulation depth M; (b) ratios J_1/J_2 (——) and J_2/J_1 (——) depending on the modulation depth M.

ADCs are recorded in RAM, and the obtained density values are stored in the FPGA internal memory (in this mode, the maximum duration of the recording cycle is 30 ms). The oscillographic mode is used mainly for debugging the device and processing algorithms.

Digital Processing Node

The FPGA was chosen as a basis for the digital node because of a high parallel computing power of matrices, which is necessary for receiving a data stream from two ADCs at 256 Mb/s with their simultaneous real-time processing. The phase shift extraction algorithm described in the previous section was translated to the Verilog hardware description language [11] and implemented in the digital phasemeter node.

Let us consider some features of this implementation. According to (10), in order to reconstruct the phase shift $\Delta\varphi$, it is necessary to calculate the ratio $\dfrac{V_\Omega(t)}{V_{2\Omega}(t)}$, multiply it by the value J_2/J_1, and calculate the arctangent. However, dividing $|V_\Omega(t)|$ by $|V_{2\Omega}(t)|$ reduces the accuracy of the final result approximately by a factor of 2 (in the case where the number of bits of the quotient coincides with the number of bits of the dividend and the divisor). Therefore, we transform expression (10) into

$$\frac{J_1(M)}{J_2(M)} V_{2\Omega}(t) = V_\Omega(t)\left|\cot(\Delta\varphi)\right|. \tag{12}$$

The ratio $\dfrac{J_1(M)}{J_2(M)}$ can be found through $\dfrac{J_1(M)}{J_3(M)}$, as was shown. Instead of running a separate memory with values $\dfrac{J_1(M)}{J_3(M)}$ in order to find the modulation depth M, it is possible to use the values $\dfrac{J_1(M)}{J_3(M)}$ as the address of the memory containing the ratio $\dfrac{J_1(M)}{J_2(M)}$. The graphs of all four ratios as a function of the modulation depth M are shown in Fig. 3.

The preferred situation is when a linear function is stored in memory. In this case, the minimum number of significant bits in a memory cell is required, so that different values of the address correspond to different values of the function. Figure 4 shows four possible memory indexing variants. The most linear dependences are J_1/J_2 on J_1/J_3 and J_2/J_1 on J_3/J_1. For substitution into expression (12), the dependence J_1/J_2 on J_1/J_3 is preferable.

Upon calculating the left-hand side of expression (12), we find $|V_\Omega\cot(\Delta\varphi)|$. In order to find $\Delta\varphi$, we mentally construct a vector with coordinates ($|V_\Omega\cot(\Delta\varphi)|$, $|V_\Omega|$) (Fig. 5, solid blue line). The obtained vector lies at an angle $\Delta\varphi$ to the x axis. This angle can be found using an iterative algorithm popular in digital electronics called CORDIC (COordinate Rotation DIgital Computer), which makes it possible to convert the Cartesian coordinates of the vector to polar coordinates, i.e., calculate the vector amplitude and the angle between it and the coordinate axis. At the very beginning, the vector is reflected so that it lies in quadrant I or IV, if necessary. Then the vector is succes-
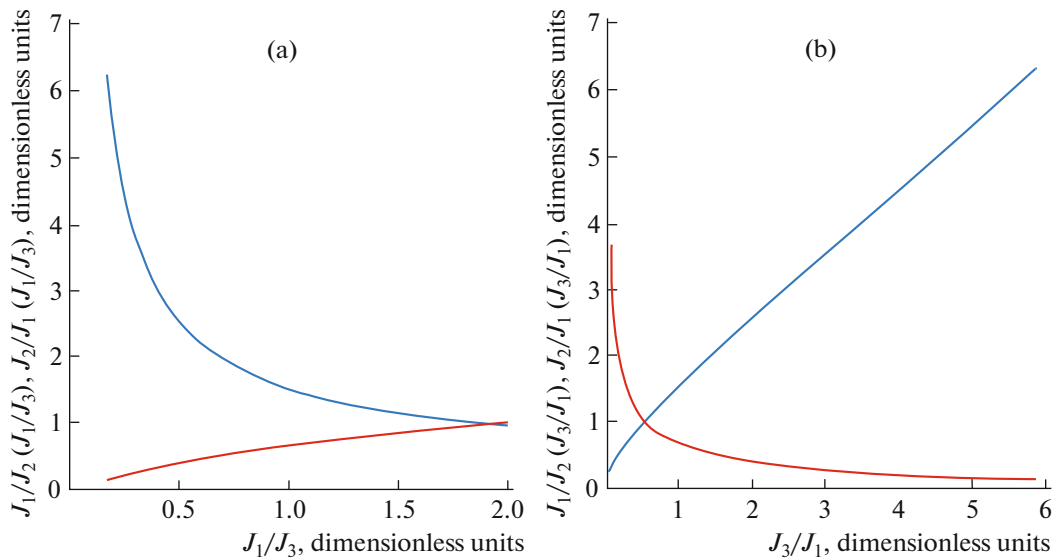
Fig. 4. (a) Ratios J_1/J_2 (———) and J_2/J_1 (———) as a function of J_1/J_3; (b) ratios J_1/J_2 (———) and J_2/J_1 (———) as a function of J_3/J_1.

sively rotated either positively or negatively depending on the sign of y. The rotation angle decreases by about a factor of 2 at each iteration (see Fig. 5). When the desired accuracy is achieved, the algorithm is stopped. The resulting new coordinate x is the amplitude of the vector, and $\Delta\varphi$ is its angle. Mathematically, this is expressed in the following relations:

$$x_{i+1} = x_i - \sigma y_i \Delta 2^{-i};$$

$$y_{i+1} = \sigma x_i 2^{-i} + y_i;$$

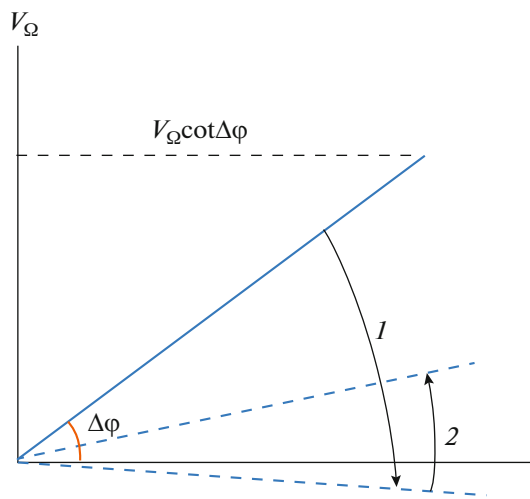$$\Delta\varphi_{i+1} = \Delta\varphi_i - \sigma\gamma_i;$$

Fig. 5. Use of the CORDIC algorithm to find the angle $\Delta\varphi$: (*1*, *2*) iteration number of the vector rotation with initial coordinates ($|V_\Omega \cot(\Delta\varphi)|$, $|V_\Omega|$). Arrows show the vector rotation direction.

$$\gamma_i = \arctan(2^{-i});$$

$$\sigma = \begin{cases} 1, & \text{if} \quad y_i < 0, \\ -1, & \text{if} \quad y_i > 0. \end{cases}$$

The advantage of this algorithm is that it uses only addition and shift operations, which makes it possible to implement it on platforms that do not support floating-point operations (which include most low-cost FPGAs).

Figure 6 shows a block diagram of the FPGA-based implementation of the described procedures:

— The amplitudes of the first three harmonics of the photodetector signal (V_Ω, $V_{2\Omega}$, $V_{3\Omega}$) are calculated from the ADC samples for the modulation signal period using the FT1, FT2, FT3 modules.

— The amplitude of the first harmonic is divided by the third one ($V_\Omega/V_{3\Omega}$) in the DIV13 module.

— On the basis of the obtained ratio, the modulation depth M is determined, which is used to select the appropriate value of the J_1/J_2 ratio from a pregenerated table stored in the ROM memory matrix.

— The amplitude of the second harmonic and the J_1/J_2 ratio selected from the ROM are fed to the input of the multiplier, which calculates the phase cotangent value $\Delta\varphi$ (with a multiplier V_Ω).

— The phase shift $\Delta\varphi$ is calculated using the CORDIC algorithm.

After performing all the above procedures, it is necessary to determine the quadrant in which $\Delta\varphi$ is located. Since expression (12) includes not the cotangent function but its modulus, the corresponding arctangent looks like the one in Fig. 7. It can be seen that the range from 0 to 2π contains four identical
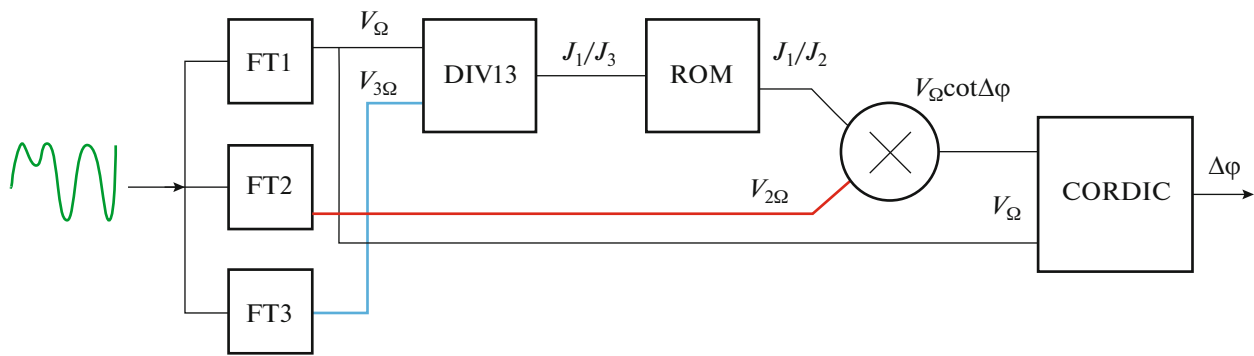
Fig. 6. Block diagram of the phase extraction algorithm in the FPGA.

branches, which differ in vertical shift and sign. When calculating the phase using the previously described algorithm, the phase is determined by the lower branch. If the phase obtained by the algorithm lies in quadrant III (according to the definition from Table 1), 180° should be added to it. If the phase is in quadrant II or IV, it is necessary to change the sign to minus and add 180° or 360°, respectively.

RESULTS AND TESTS

Algorithm Robustness to Noise

The algorithm described in [6] and operating in the amplitude–time domain uses a single value of the signal amplitude per modulation period to calculate the phase shift, while the algorithm operating in the frequency domain uses all the obtained values of the photodetector signal amplitudes per period. The number of such values is determined by the sampling rate of the ADC used to digitize the signals. As a result, the

higher the sampling rate, the higher the robustness of the considered algorithm to noise.

This assertion is based on the following. In the Fourier transform, each signal value has a noise component, which is some random variable with distribution parameters $\mu = 0$, $\sigma = \sigma_n$, where μ is the mathematical expectation, and σ is the standard deviation. Owing to the central limit theorem, the standard deviation of the average noise value in a harmonic is
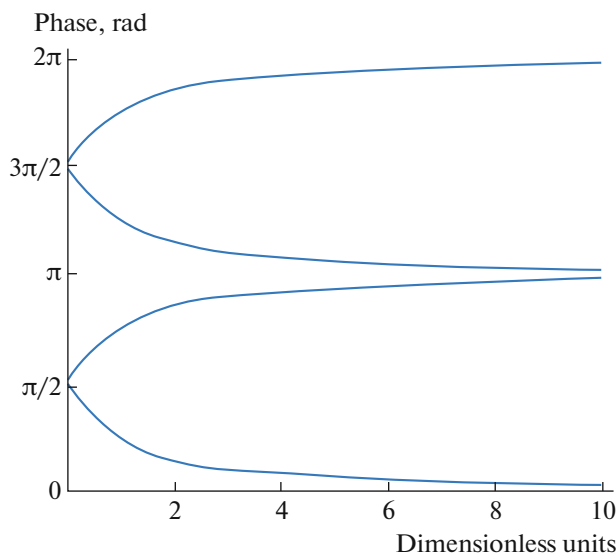

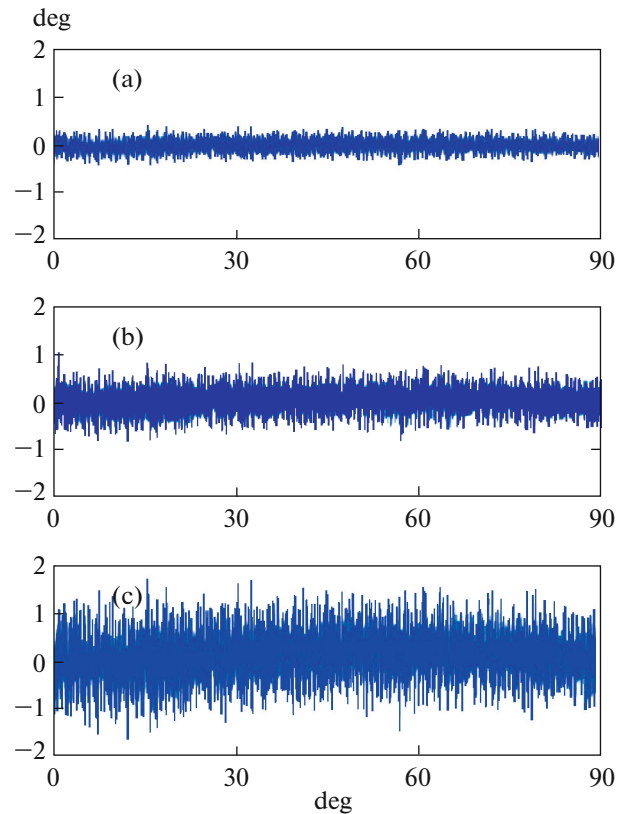**Fig. 7.** Arctangent modulus graphs.

Fig. 8. Phase deviation from the expected value in the range of the phase change from 0° to 90° for noise amplitudes of (a) 1, (b) 2, and (c) 4% of the ADC scale.
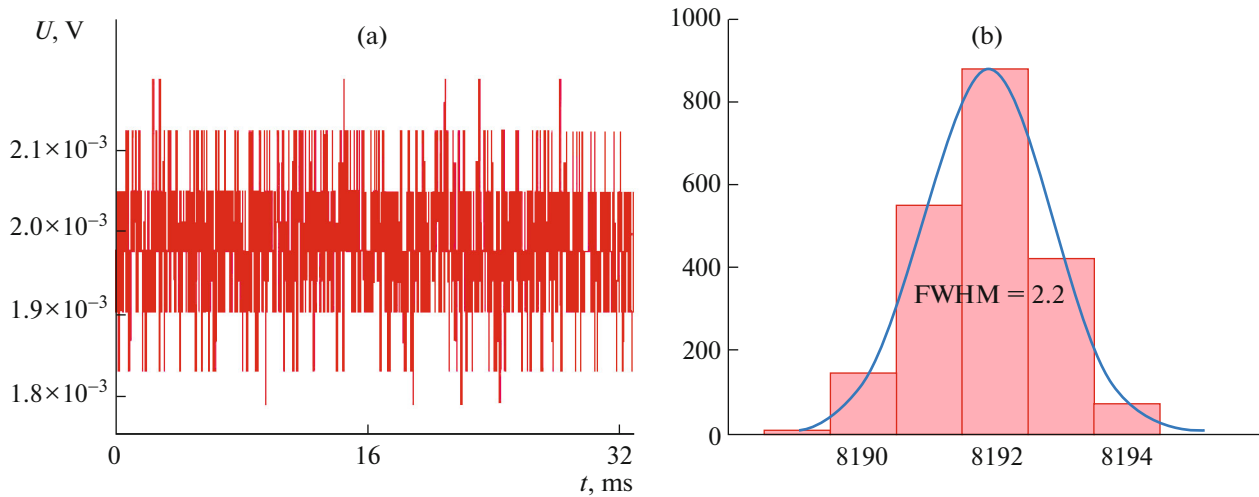
Fig. 9. (a) Oscillogram of the output signal in absence of the signal at input; (b) amplitude distribution of the noise component (along the horizontal axis, the ADC code; along the vertical axis, the number of ADC code displays; FWHM is the full width at half maximum).

$\sigma_n/\sqrt{2N}$, where N is the number of values (in our case, for the ADC sampling rate of 64 MHz $N = 256$). The presence of the number 2 is explained by the fact that each random variable enters the Fourier transform with a different weight proportional to some sine value.

In order to verify this proposition, a simulation was performed using noisy signals. The superimposed noise was modeled by a Gaussian distribution with zero expectation and standard deviation of 1, 2, and 4% of the full ADC scale.

Plots of the deviation of the phase shift from the expected value in the range from 0° to 90° are shown in Fig. 8. The mean square deviations are 0.11°, 0.23°, and 0.46° for noises with amplitudes of 1, 2, and 4%, respectively. As can be seen, the algorithm is indeed very stable, which is confirmed by the absence of jumps in the change in phase shift values. The mean square deviation of the result is linearly related to the
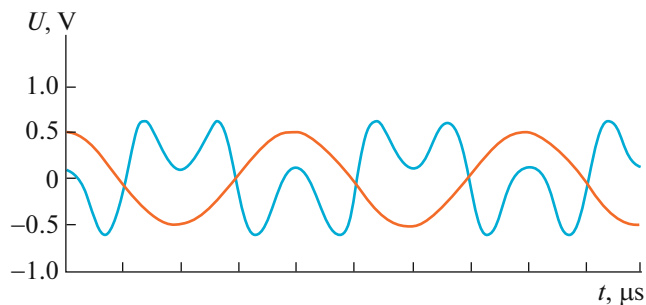

Fig. 10. External oscillator output signals (oscilloscope image: one cell horizontally = 1 μs): (——) simulated photodetector signal and (——) simulated modulator signal.

amplitude of the superimposed noise. Moreover, by averaging the noise over all points of the period, its effective value decreases by an order of magnitude. Therefore, for the relative amplitude of the original signal noise of 1%, the relative error of the phase determination is only 0.1%.

Measurement Module Test

In order to estimate the intrinsic noise level of the phasemeter, measurements were performed in the oscillographic mode of the device and in the absence of a signal at the input. Figure 9a shows the noise oscillogram and Fig. 9b shows the corresponding histogram of the noise component amplitude distribution. Its half-width is 2.2 low-level bits of the ADC, which corresponds to 0.01% of the full scale of the 14-bit ADC (the full scale of ADC corresponds to a signal level of 2 V). According to the previous calculations, it can be seen that such a level of intrinsic noise of the phasemeter does not affect the results of measurements of the $\Delta\varphi$ phase.

In order to test the measurement module, signal (5) simulating the photodetector signal was fed to it using an arbitrary waveform generator (the blue contour in Fig. 10). This signal was modulated linearly with increasing or decreasing phase at each period. The $M\sin(\Omega t)$ signal simulating the modulator signal (gold contour in Fig. 10) was also applied to the input of the measurement module.

Figure 11 shows the results of testing the performance of the algorithm with a linear variation of the phase shift $\Delta\varphi$ from 0° to 720° in steps of 5°. The horizontal axis represents the phase shift and the vertical axis represents the measurement results of the phasemeter. In order to verify that the phasemeter is inde-
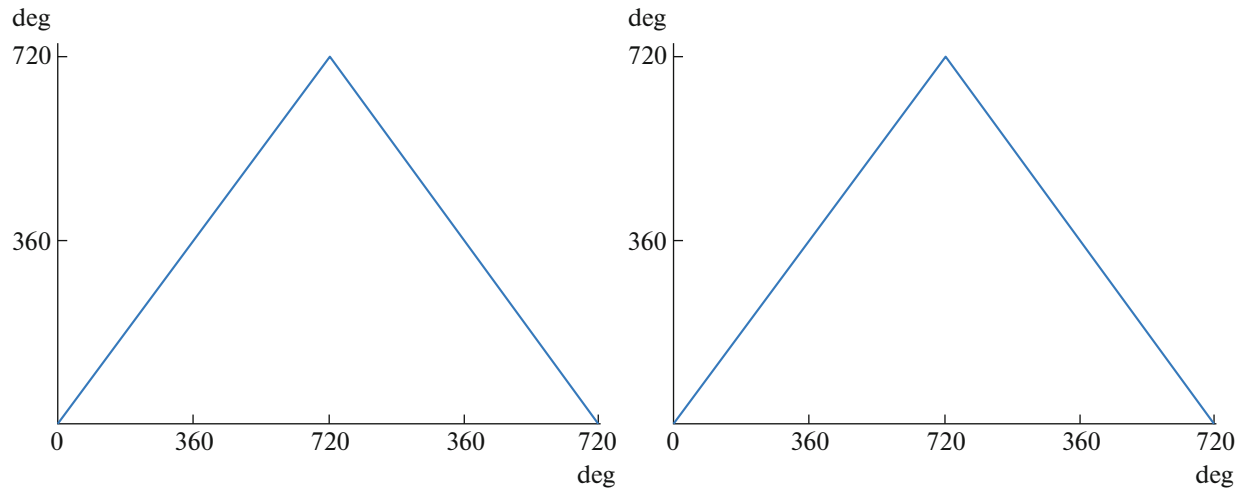
Fig. 11. Results of the algorithm test under a linear phase shift from 0° to 720° and back with step of 5°: the horizontal axis is the given phase shift; the vertical axis is the phase shift measured with a phasemeter. Input signal modulation depth is (a) $\pi/2$ and (b) π radians.
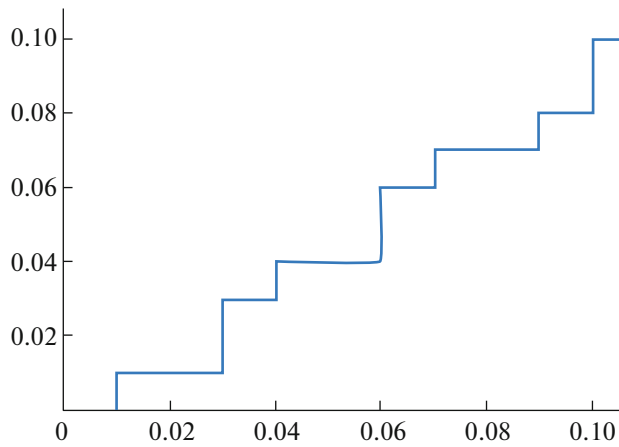

Fig. 12. Estimation of the resolution of the phasemeter with a linear phase shift in the range from 0° to 0.1° with step of 0.01°: the given phase shift is plotted on the horizontal axis; the phase shift measured by the phasemeter is plotted on the vertical axis.

Fig. 13. Photographs of the measurement module of the dispersion interferometer.

pendent of changes in modulation depth in the range from $\pi/2$ to π, signals with a modulation depth of (b) π and (a) $\pi/2$ were fed to the input of the phasemeter. It can be seen that the results were identical, which proves the robustness of the algorithm to changes in the modulation depth within a given range.

Figure 12 shows the output signal of the phasemeter at a linear phase shift $\Delta\varphi$ with a step of 0.01°, corresponding to a linear plasma density 4×10^{11} cm^{-2} in the range of 0.1°. The horizontal axis is the phase setpoints, and the vertical axis is the measured phase.

Photographs of the finished DI measurement module are shown in Fig. 13.

CONCLUSIONS

A measurement module of a dispersion interferometer based on a CO_2 laser was developed, which makes it possible to reconstruct the linear plasma density with a time discreteness of 4 μs/count and a resolution of 4×10^{11} cm^{-2}. The algorithm for calculation of the plasma density implemented in the digital node is based on the harmonic analysis of the interferometer signals and is robust to noise and changes in the modulation depth. Such characteristics of the device make it possible to use the results of its measurements in the feedback loops for plasma density control, in particular, for the system of monitoring and automatic control of plasma density at the Globus-M2 installation (St. Petersburg, Russia).

CONFLICT OF INTEREST

The authors declare that they have no conflicts of interest.

REFERENCES

1. A. L. Solomakhin, P. A. Bagryanskii, R. V. Voskoboinikov, P. V. Zubarev, A. N. Kvashnin, A. A. Lizunov, V. V. Maksimov, and A. D. Khil'chenko, Instrum. Exp. Tech. **48**, 649 (2005).

2. S. Bozhenkov, G. Fuchert, H. Niemann, M. Beurskens, Y. Feng, O. Ford, J. Geiger, M. Hirsch, U. Hoefel, M. Jakubowski, J. Knauer, P. Kornejew, A. Langenberg, H. Laqua, H. Maassberg, et al., in *Proceedings of the 43rd EPS Conference on Plasma Physics, 2016,* vol. 40A, p. O2.106.

3. T. Akiyama, R. Yasuhara, K. Kawahata, K. Nakayama, S. Okajima, K. Urabe, K. Terashima, and N. Shirai, J. Instrum. **10**, P09022 (2015).

4. H. Dreier, P. Bagryansky, N. Baumgarten, W. Biel, H. T. Lambertz, M. Lehnen, A. Lizunov, and A. Solomakhin, Rev. Sci. Instrum. **82**, 063509 (2011).

5. A. Lizunov, P. Bagryansky, A. Khilchenko, Yu. V. Kovalenko, A. Solomakhin, W. Biel, H. T. Lambertz, Yu. Krasikov, M. Mitri, B. Schweer, and H. Dreier, Rev. Sci. Instrum. **79**, 10E708 (2008).

6. A. D. Khil'chenko, A. N. Kvashnin, S. V. Ivanenko, P. V. Zubarev, D. V. Moiseev, and Yu. V. Kovalenko, Instrum. Exp. Tech. **52**, 382 (2009).

7. T. J. Tayag and R. C. Watson, *Digital Demodulation of Interferometric Signals, Modern Metrology Concerns* (InTech, Rijeka, 2012), p. 317.

8. V. B. Minaev, V. K. Gusev, N. V. Sakharov, V. I. Varfolomeev, N. N. Bakharev, V. A. Belyakov, E. N. Bondarchuk, P. N. Brunkov, F. V. Chernyshev, V. I. Davydenko, et al., Nucl. Fusion **57** (6) (2017).

9. A. L. Solomakhin, Cand. Sci. (Phys. Math.) Dissertation (Budker Inst. Nucl. Phys. Sib. Branch of RAS, 2006).

10. V. Zaveryaev et al., in *Fusion Physics* (IAEA, Vienna, 2012), p. 360.

11. *IEEE Standard for Verilog Hardware Description Language* (IEEE, 2006).

Translated by O. Pismenov